

ViewDelta: Text-Prompted Change Detection in Unaligned Images

Subin Varghese

University of Houston

4302 University Dr, Houston, TX 77004

srvargh2@cougarnet.uh.edu

Joshua Gao

University of Houston

4302 University Dr, Houston, TX 77004

jkgao@cougarnet.uh.edu

Vedhus Hoskere

University of Houston

4302 University Dr, Houston, TX 77004

vhoskere@central.uh.edu

Abstract

Detecting changes between images is a fundamental problem in computer vision with broad applications in situational awareness, infrastructure assessment, environment monitoring, and industrial automation. Existing supervised models are typically limited to detecting specific types of changes, necessitating retraining for new tasks. To address these limitations with a single approach, we propose a novel change detection method that is the first to utilize unaligned images and textual prompts to output a binary segmentation of changes relevant to user-provided text. Our architecture not only enables flexible detection across diverse change detection use cases, but also yields state-of-the-art performance on established benchmarks. Additionally, we release an accompanying dataset comprising of 100,311 pairs of images with text prompts and the corresponding change detection labels. We demonstrate the effectiveness of our method both quantitatively and qualitatively on datasets with a wide variety of viewpoints in indoor, outdoor, street level, synthetic, and satellite images. [GITHUBPAGELINKHERE](#)

1. Introduction

Detecting and understanding changes between snapshots of our world in the form of images is a critical problem in computer vision [4, 6, 18, 42], with wide-ranging applications including situational awareness [12, 53], infrastructure damage assessment [38, 41, 44, 50], and environmental monitoring [16, 30], among others.

Traditional change detection methods analyze two images of the same scene to identify differences, but they are generally limited to specific types of changes and data domains on which they were trained (e.g., detecting building

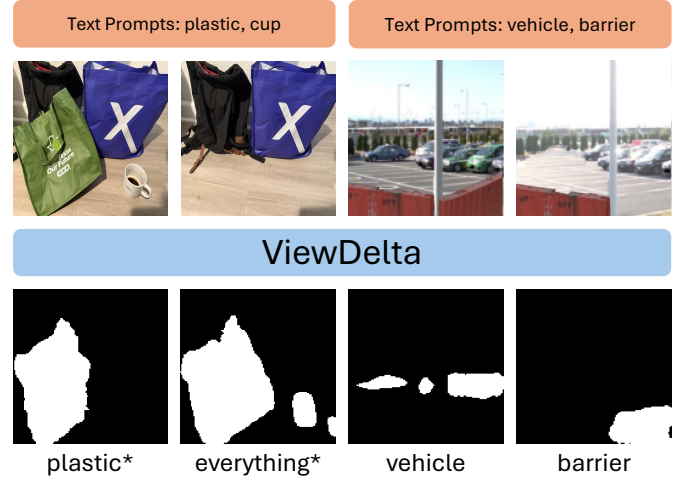


Figure 1. Given a pair of aligned or unaligned images before and after an event as well as a text prompt of what change is relevant to a user, ViewDelta outputs a segmentation of the desired change. The prompts "plastic" and "everything" are example text prompts the model has generalized to understand and does not appear in the dataset.

changes in satellite imagery). This is particularly problematic for users that are interested in only specific types of changes that fall outside of how change was defined in other datasets. Additionally, most existing methods assume precise alignment between images, making them very sensitive to camera pose variations. This assumption results in limited applicability in real-world scenarios, where images are frequently taken from slightly different viewpoints or with differing orientations, resulting in poor performance when images are not perfectly aligned.

To address these limitations, we propose a novel ap-

proach, shown in Fig. 1, that enables user-defined prompt-driven change detection that remains robust even with unaligned image pairs and text prompts not seen during training. Our method, ViewDelta, allows users to use natural language prompts to specify the types of changes they care about, making the system adaptable to a wide variety of applications. This customization allows a single model to generalize effectively across diverse domains—including street-level and satellite imagery—without requiring domain-specific retraining or multiple specialized models. By consolidating these capabilities into one model, our approach provides a data scalable, versatile solution compared to traditional methods, with added robustness to image alignment issues.

To support this model, we introduce a new dataset, CSeg, designed specifically for prompt-driven change detection with unaligned images from various types of imagery. This dataset leverages inpainting techniques to create realistic change pairs, avoiding the labor-intensive task of manually labeling thousands of images with targeted changes. Our dataset also incorporates “red herring” changes to prevent the model from learning inpainting artifacts as change, further enhancing its ability to generalize to unaligned real-world images.

Our experiments demonstrate that ViewDelta, with its prompt-driven capability and change detection architecture, competes with traditional methods fine-tuned for specific domains and aligned images. This performance is consistent across indoor, outdoor, street-level, synthetic, and satellite imagery, underscoring its broad applicability and effectiveness. Our contributions are as follows.

- We introduce a new change detection task for detecting changes in images by allowing users to describe what change is relevant to them with text and outputting a binary segmentation of the change if it exists.
- We propose ViewDelta, the first transformer-based neural network architecture for prompt guided change detection.
- We create and release a new dataset of both aligned and unaligned image pairs with text descriptions and change masks to support research in this area.
- We develop the first change detection model effective across diverse image types—including indoor, outdoor, street-level, synthetic, and satellite imagery—without requiring retraining or separate model versions.
- ViewDelta competes with state-of-the-art fine-tuned dataset-specific models.

2. Related Work

Change Detection: Change detection (CD) entails identifying variations between two images, I_a and I_b , captured at different times and potentially from different viewpoints, producing a binary change map $M \in \{0, 1\}^{H \times W}$ that indicates altered regions. Traditional CD methods have largely

focused on 2D image pairs with minimal or no viewpoint changes, as commonly seen in applications such as surveillance and satellite imagery [3, 14, 15, 56]. More recent approaches have extended CD to complex 3D settings, where the camera poses of I_a and I_b may vary significantly, and even to inherently 3D data like point clouds [1, 27, 37, 46]. This shift toward viewpoint variability introduces additional challenges, particularly in accurately annotating changes under varying viewpoints, which makes manual annotation costly and complex.

To address the difficulties associated with labeling under variable viewpoints, some methods leverage synthetic data or 3D representations. However, these advancements have been constrained by a lack of large-scale, real-image datasets annotated for CD with viewpoint variation. Consequently, models trained in these scenarios are often limited to synthetic data or rely on 3D modalities restricting the potential use cases to only scenarios where 3D data is available. This creates a need for real-image CD models robust enough to handle diverse viewpoints. To address this gap, we leverage three datasets. For the first dataset, we use the PSCD dataset [39] which consists of shifted panoramic images that, when cropped, shows slight variation in views. For the second dataset, we use the SYSU-CD [40] dataset which consists of fixed view satellite imagery. Finally to expand the models vocabulary and introduce more variation to view, we create CSeg, a dataset consisting of multi-view real images with multiple inpainted changes.

Semantic Change Detection: Unlike traditional CD, Semantic Change Detection consists of multiple categories of changes that must be selected similarly to semantic segmentation [9, 43, 52]. Given I_a and I_b , the objective of semantic change detection is to predict a semantic segmentation map $S \in \{1, 2, \dots, N\}^{H \times W}$, where N is the total number of semantic classes. Each pixel $S_{i,j}$ is assigned a class label $c \in \{1, 2, \dots, N\}$, identifying the type of semantic change corresponding to that region. Semantic change detection has been successfully applied to various types of imagery, including satellite [52], street view [39], and warehouse [32] images. However, current methods are typically tailored to specific domains, and a unified model that can generalize across different categories within a single saved checkpoint does not yet exist. With ViewDelta due to our unique formulation of CD with a text prompt, we are able to jointly train on multiple datasets and create a single saved model that achieve state of the art performance rather than a finetuned model for each dataset.

Open Vocabulary Image Segmentation: Open Vocabulary Image Segmentation is a computer vision task that involves labeling each pixel with categories beyond a predefined set, including categories potentially unseen during training [28, 29, 55]. This flexibility is achieved through models that associate text and image features, often utilizing

vision-language frameworks like CLIP [33], which align visual and textual embeddings within a shared space. Our approach builds on these methods by integrating text and image models to enhance change detection. Rather than highlighting all possible changes, our model interprets a user-provided text prompt to selectively highlight changes relevant to the specified user text. Additionally, we train on an “all” prompt, enabling users to view all detected changes if desired.

3. Architecture

In this section, we introduce **ViewDelta**, our proposed architecture for text-prompted change detection, as illustrated in Fig. 2. ViewDelta processes two input images, I_a and I_b , captured before and after a change event, respectively, along with a text prompt T that specifies the type of change relevant to the user. The goal is to predict a binary segmentation map $M \in \{0, 1\}^{H \times W}$, where $M_{i,j} = 1$ indicates the presence of the specified change at pixel location (i, j) and $M_{i,j} = 0$ otherwise.

The architecture comprises of several key components: text tokenization to convert the text prompt T into a sequence of tokens, image tokenization for generating token representations of I_a and I_b , a fusion layer for combining text and image tokens, a transformer backbone for joint feature representation, and an MLP-based segmentation head to produce the final binary map M . This design enables ViewDelta to selectively identify and highlight regions that align with the specified text prompt, providing a flexible and user-focused approach to change detection.

3.1. Text Tokenization

We leverage only the text encoder of the SigLip [54] model due to its improved performance against models such as CLIP [33], OpenCLIP [13], and EVA-CLIP [45]. We leave the SigLip model frozen in order to keep the text generalization ability of SigLip. This way even with a limited number of varying texts in the dataset the model may still understand unseen words. From the SigLip text encoder we extract 64 tokens which are then fed into a layer we shall refer to as the Token Convolution layer to upsample the number of tokens from 64 to 68 and downsample the token dimension to 512 to make the text token dimensions compatible with the preceding networks in ViewDelta. The Token Convolution network leverages two 1D convolution layers and a final linear layer. The architecture of the Token Convolution network can be seen in Fig. 3.

3.2. Image Tokenization

Smaller patch sizes have been shown to improve the performance of transformer based models for dense prediction tasks such as semantic segmentation [26, 49, 51]. As such, we take the same approach implemented by Segformer [51]

(Overlapping Patch Embedder) and use a 2D convolution with a kernel size of 7, stride of 3, and padding of 3 to generate many patches of an input image. We use a single Overlapping Patch Embedder to generate tokens for both I_a and I_b . While two different Overlapping Patch Embedders could be used, from our initial experimentation, we have found that tokens corresponding to one embedder tended to outweigh the other causing artifacts. Though this artifacting stabilized once convergence was achieved, no strong improvements to the performance of the model was shown. We opt to keep only a single Overlapping Patch Embedder for a more compute efficient network design.

3.3. Fusing Text and Image Tokens

To address the observed instability during training when simply concatenating text and image tokens in the ViewDelta architecture, we introduce a **Text and Image Token Fusion Layer**. This layer re-weights the tokens, aligning them into a similar feature space, before further processing. The Fusion layer operates as follows:

1. **Token Normalization:** Each set of tokens, \mathbf{T}_A (Image A), \mathbf{T}_B (Image B), and \mathbf{T}_{text} (text), is processed through a separate RMSNorm layer with learnable weights to align token distributions for improved compatibility:

$$\hat{\mathbf{T}}_A = \text{RMSNorm}_A(\mathbf{T}_A)$$

$$\hat{\mathbf{T}}_B = \text{RMSNorm}_B(\mathbf{T}_B)$$

$$\hat{\mathbf{T}}_{\text{text}} = \text{RMSNorm}_{\text{text}}(\mathbf{T}_{\text{text}})$$

2. **Token Concatenation:** The normalized tokens are concatenated along the feature dimension to form a combined token set, $\mathbf{T}_{\text{combined}}$:

$$\mathbf{T}_{\text{combined}} = \text{concat}(\hat{\mathbf{T}}_A, \hat{\mathbf{T}}_B, \hat{\mathbf{T}}_{\text{text}})$$

3. **Projection through MLP:** The concatenated tokens are fed into a three-layer MLP with a SiLU activation function, inspired by the FeedForward network in the Llama 3 transformer architecture. The MLP re-weights and fuses the token representations to ensure compatibility in the final feature space.

For an input token vector \mathbf{x} , the MLP operation is defined as:

$$\mathbf{y} = \mathbf{W}_2 (\text{SiLU}(\mathbf{W}_1 \mathbf{x}) \odot \mathbf{W}_3 \mathbf{x})$$

where $\mathbf{W}_1 \in \mathbb{R}^{d \times h}$, $\mathbf{W}_2 \in \mathbb{R}^{h \times d}$, and $\mathbf{W}_3 \in \mathbb{R}^{d \times h}$ are the learnable weight matrices, with d being the input and output dimension, and h the hidden dimension determined by the MLP structure.

This fusion process re-weights and combines the tokens, mitigating the instabilities and convergence issues observed in initial experiments, and provides a unified representation compatible with the transformer backbone and segmentation head.

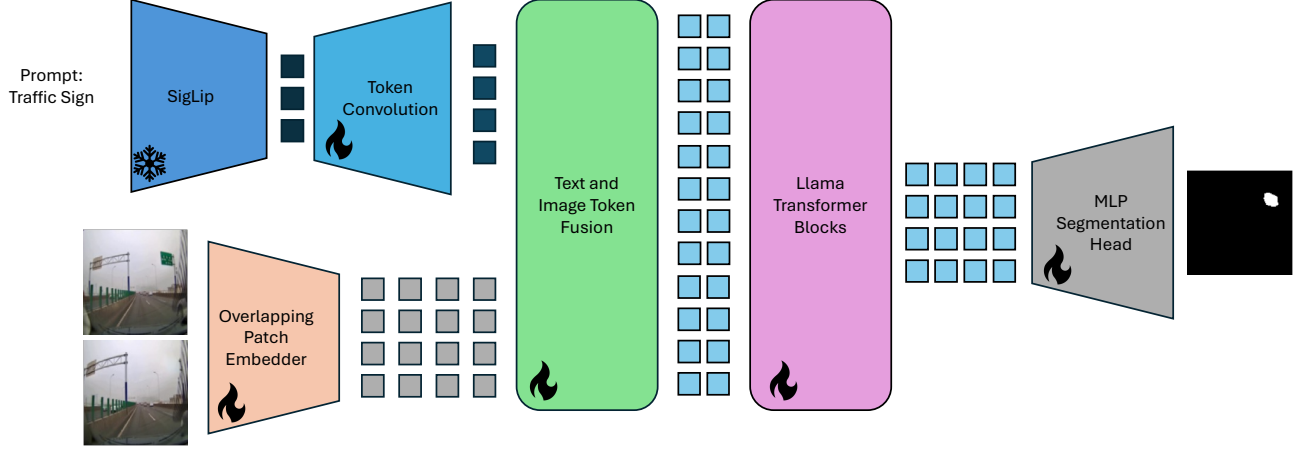


Figure 2. Overview diagram of the ViewDelta architecture consisting of two primary branches to process images and text before a fusion layer. This is followed by 16 Llama transformer blocks and an MLP Segmentation Head.

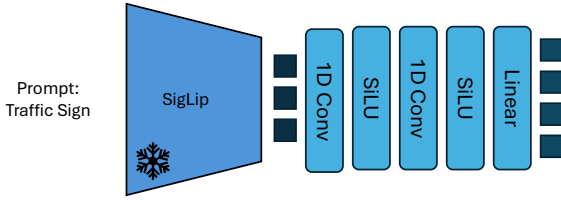


Figure 3. Architecture of the Token Convolution network that processes 64 tokens from the SigLip text encoder, upsampling them to 68 tokens and downsampling the token dimension to 512 using two 1D convolution layers and a linear layer.

3.4. Backbone

We adopt a scaled-down version of the Llama 3 transformer architecture [10] as our backbone model, selected for its efficient design and proven performance. To tailor the architecture to our multimodal setting, we implement several modifications:

1. **Unmasked Attention:** We remove masking within the transformer blocks, enabling attention across all tokens regardless of their source. This change allows the model to capture global dependencies among tokens from both images and text, facilitating comprehensive feature integration.
2. **Reduced Depth:** We scale down the transformer to 16 layers. This reduction strikes a balance between computational efficiency and model capacity, making it suitable for our application without compromising performance.
3. **Grouped Query Attention :** We opt not to use grouped query attention [2], as our model produces the complete output from a single inference per input pair (I_a , I_b , and T).
4. **Activation Function:** We replace the original activation function with the SiLU activation function [11],

which we find demonstrated improved convergence in ViewDelta.

3.5. MLP Segmentation Head

The MLP Segmentation Head in ViewDelta is designed to transform the fused token representations from the backbone transformer into a dense prediction suitable for segmentation tasks. Our segmentation head leverages MLPs to aggregate features and produce a segmentation map.

Input Reshaping: The fused tokens output by the backbone transformer have the shape $\mathbf{T}_{\text{fused}} \in \mathbb{R}^{B \times S \times E}$, where B is the batch size, S is the sequence length, and E is the embedding dimension. We first reshape these tokens into a feature map suitable for dense prediction. Assuming the tokens represent a square spatial arrangement, we compute the height and width as $H = W = \sqrt{S}$. The tokens are then reshaped to form a feature map $\mathbf{X} \in \mathbb{R}^{B \times E \times H \times W}$.

Hierarchical Feature Extraction: Inspired by the efficiency of Segformer, we employ a similar architecture to their All-MLP Decoder. We leverage four linear layers, each processing a progressively deeper feature map to extract features at different levels. The linear layers operate solely on the embedding dimension and not the spatial dimension, allowing the segmentation head to remain lightweight and enabling more computational resources for the backbone network.

Let X represent the final output from the backbone transformer network. We feed X into the first linear layer and record its output feature map. This output is then passed through an activation function before being fed into the next linear layer. This process is repeated through four linear layers, resulting in four feature levels. These levels are subsequently upsampled and concatenated to form the final feature representation.

1. Feature Projection through Linear Layers:

Let the feature map at each level i be denoted as F_i . We initialize by feeding X into the first linear layer L_1 :

$$F_1 = \text{Activation}(L_1(X))$$

Then, we iteratively pass each output F_i through the next linear layer L_{i+1} :

$$F_{i+1} = \text{Activation}(L_{i+1}(F_i))$$

where $i = 1, 2, 3$ until we reach F_4 , the final feature level.

2. Upsampling and Concatenation:

Each feature level F_i is upsampled to a common spatial size (H, W) using bilinear interpolation:

$$\tilde{F}_i = \text{Upsample}(F_i, \text{size} = (H, W), \text{mode} = \text{"bilinear"})$$

The upsampled feature maps $\{\tilde{F}_1, \tilde{F}_2, \tilde{F}_3, \tilde{F}_4\}$ are then concatenated along the channel dimension:

$$F_{\text{concat}} = \text{Concat}(\tilde{F}_1, \tilde{F}_2, \tilde{F}_3, \tilde{F}_4) \in \mathbb{R}^{H \times W \times 4D}$$

3. Dimensionality Reduction through Convolutions:

The final concatenated feature map F_{concat} is then passed through two 2D convolution layers to progressively reduce the embedding dimension. The first convolution reduces the dimension to $D/4$, and the second convolution reduces it further to 2 for binary segmentation:

$$F_{\text{reduced}} = \text{Conv}_2(\text{Conv}_1(F_{\text{concat}}))$$

where:

- $\text{Conv}_1 : \mathbb{R}^{H \times W \times 4D} \rightarrow \mathbb{R}^{H \times W \times \frac{D}{4}}$
- $\text{Conv}_2 : \mathbb{R}^{H \times W \times \frac{D}{4}} \rightarrow \mathbb{R}^{H \times W \times 2}$

This hierarchical feature extraction allows for efficient multi-level feature aggregation while keeping the segmentation head lightweight.

3.6. Implementation Details

PSCD view variation: The PSCD dataset comprises of 770 panoramic image pairs captured in a suburban environment. Though the PSCD dataset was originally released for view aligned change detection of panoramic images, from further inspection, we have found that, when zoomed in, the dataset was found to have some varying amounts of viewpoint change. To leverage this data as a source of real street level change detection we take each panoramic image and extract non-overlapping crops of size 256×256 . However, the viewpoint variation between images is still less significant than desired, and future work will focus on expanding this aspect. The labels provided by PSCD are originally intended for semantic segmentation across classes such as vehicles and people. We use these classes to generate several binary segmentation masks, with each class serving as a distinct text prompt for segmentation.

Training Details: To effectively train ViewDelta on multiple datasets jointly, we utilize the Adam optimizer [20] with a one-epoch warm-up and a cosine annealing learning rate decay, starting at a learning rate of 2×10^{-5} . Training is conducted with a batch size of 3 across 4 GPUs, yielding an effective total batch size of 12.

4. CSeg Dataset

A major factor contributing to the recent advancements in deep learning is the accessibility of large-scale datasets with high-quality annotations. To the best of our knowledge, there is currently no existing dataset that contains image pairs with text-guided change masks, especially those that involve view shifts. Even though the processed PSCD dataset provides minor view alignment differences, it is limited to traffic-like classes such as “vehicles”, “barrier”, “human”, and “lane marking”. A dataset is required with significantly more classes and corresponding text prompts of the class to expand ViewDelta’s vocabulary. However, manually labeling thousands of image pairs with changes is cumbersome, expensive, and impractical to scale. Inspired by the COCO-Inpainted dataset [37], we propose a procedure that leverages the large-scale video dataset, SAV [34], and the image inpainting model, LaMa [47], to generate CSeg: a realistic, varying-view, and text-guided change detection dataset.

In the following sections, we describe each component of our pipeline, shown in Fig. 4, to create CSeg. This pipeline requires two frames from a video in the SAV dataset as the input. We first select a Frame A and Frame B within a SAV dataset video, and leverage Gemini 1.5 Flash’s [48] vision capabilities to propose a COCO class that exists in Frame A to be the text prompt. We then provide Frame A, Frame B, and the text prompt to Grounded SAM 2 [19, 21, 35, 36] to collect tracked masks to be inpainted in order to simulate a synthetic change. Object tracked masks included in the SAV dataset are also collected and inpainted to be used as “red herring” masks to dissuade our model from learning inpainting artifacts. This results in a change mask label, I_a , I_b , and a text prompt.

4.1. Selecting Image Frame Pairs

The SAV dataset consists of videos taken by ordinary people from around the world, and due to the motion in the captured videos, the camera pose continuously changes. We use this change in camera pose over the course of a video to our advantage to create a realistic multi-view change dataset.

We select two frames, Frame A and Frame B, from a SAV video that can capture a change in view. To do so, we first select a frame in increments of 6 in each video in SAV to be Frame A. Due to potential labeling ambiguity caused by objects disappearing due to camera pose changes seen

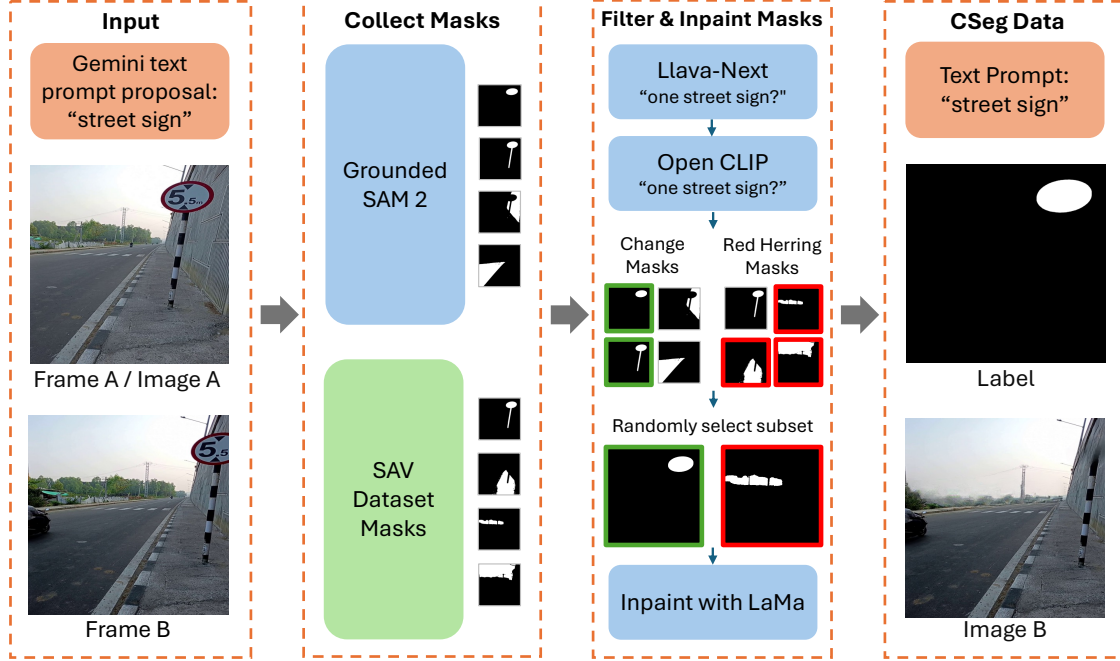


Figure 4. The above procedure is used to generate the CSeg dataset. We first select a Frame A (which will be used as Image A) and Frame B from a SAV dataset video. To generate a text prompt, we leverage Gemini to propose a COCO class that exists in Frame A. Then, we provide Frame A, Frame B, and the generated text prompt to Grounded SAM 2 to collect tracked masks to be inpainted in order to simulate a synthetic change. Object tracked masks included in the SAV dataset are also collected and inpainted to be used as “red herring” masks to dissuade our model from learning inpainting artifacts. These masks are further classified by Llava-Next and Open CLIP models to validate that the classification is correct and is a single instance of the text prompt. A random subset of the validated change mask and red herring masks are selected to be inpainted. This results in a text prompt, binary segmentation label, I_a , I_b .



Figure 5. Whether or not the girl was inpainted or if the camera simply panned to the right is ambiguous.

in Fig. 5, we aim to select a Frame B that captures a view shift without transitioning to a completely new scene. To do so, we require all instances of objects related to a generated text prompt to maintain a similar position between Frame A and Frame B. We enforce this by using Grounded SAM 2 [19, 21, 35, 36] with a low confidence threshold to track all instances of the text prompt in the SAV video, and require each of these tracked masks to have an IoU of at least 0.1 between their Frame A and Frame B masks. This ensures that the objects of interest remain in both frames A and B thus removing ambiguities. We select the frame that is farthest in time away from Frame A that meets these requirements with a maximum of 24 frames beyond Frame

A. If all Frame B candidates are insufficient, we set frames A and B to be the same frame to include image pairs with fixed view in CSeg.

4.2. Inpainted Changes

To simulate changes, we inpaint objects in Frame B. The first step is to leverage Gemini 1.5 Flash’s [48] vision capabilities to propose a COCO class that exist in Frame A to be used as our text prompt. We choose from the COCO classes [22] because it consists of common everyday objects that a user is likely to be interested in. However, we remove orange due to ambiguity between the color and the fruit. This text prompt, Frame A, and Frame B will then be provided to Grounded SAM 2 which will segment and track the all instances of objects related to our text prompt across the Frame A and Frame B. Since we use Grounded SAM 2 with a low required confidence threshold, we need to validate if each tracked mask are misclassified as the text prompt. We leverage Llava-Next [23–25] and Open CLIP models to classify all Grounded SAM 2 masks as a single instance of our text prompt and remove any mask that doesn’t correspond to our text prompt. We then inpaint Frame B with a randomly selected subset of these validated masks to simu-

Model	IoU	F1	Rec	Prec
ViewDelta	67.82	80.82	75.88	86.47

Table 1. Quantitative Results On The CSeg Dataset.

Model	mIoU	F1	Rec	Prec
CSCDNet	22.3	—	—	—
+ SSCDNet [39]	32.2	—	—	—
CSSCDNet [39]	32.2	—	—	—
ViewDelta	36.83	53.83	55.97	51.86

Table 2. Quantitative Results On The PSCD Dataset.

late change. Finally, the Frame A masks corresponding to the objects inpainted in Frame B will be added to the change mask label which will denote changes in Image A.

4.3. Combating Inpainting Noise

Although inpainting produces seemingly realistic changes, we noticed that the inpainted regions tend to have inpainting artifacts (as observed in other works in the literature [6, 7, 17]). To discourage the model from simply learning these artifacts instead of the changes between images, we inpaint “red herring” masks. These are a randomly selected subset of tracked SAV masks that are classified as not the text prompt. These tracked masks are inpainted in Frame B but are not added to the change mask. During training, this forces the model to learn the change between the two images that are consistent with text prompt rather than labeling inpainting noise as changes.

5. Experiments

To assess the effectiveness of ViewDelta, we evaluate its performance on three diverse datasets: CSeg, PSCD [39], and SYSU-CD [40]. These datasets cover a broad range of domains, including indoor, outdoor, street-view, and satellite imagery, ensuring a comprehensive evaluation across different contexts.

This section first presents quantitative metrics for each dataset, evaluating several state-of-the-art models on each dataset individually and reporting metrics such as intersection over union (IoU). Following this, we provide a qualitative analysis, showcasing examples of ViewDelta’s performance across various samples in the dataset.

5.1. Quantitative Evaluation

We quantitatively evaluate the performance of ViewDelta on three diverse datasets: CSeg, PSCD [39], and SYSU-CD [40], comparing it against several state-of-the-art methods using standard metrics, including Intersection over Union (IoU), F1 score, Recall (Rec), and Precision (Prec).

Method	IoU	F1	Rec	Prec
FC-EF [8]	60.09	75.07	75.84	74.32
FC-Siam-diff [8]	56.96	72.57	61.21	89.13
FC-Siam-conc [8]	61.75	76.35	71.03	82.54
BiDateNet [31]	62.52	76.94	72.60	81.84
STANet [5]	63.09	77.37	85.33	70.76
DSAMNet [40]	64.18	78.18	81.86	74.81
ViewDelta	67.18	80.37	77.40	83.58

Table 3. Quantitative Results on SYSU-CD Dataset

Results are summarized in Tabs. 1 to 3. On the CSeg dataset Tab. 1, ViewDelta achieves an IoU of 67.82%, an F1 score of 80.82%, a recall of 75.88% with a high precision of 86.47%. For the PSCD dataset Tab. 2, which includes viewpoint changes and challenging illumination conditions, ViewDelta competes with CSCDNet+SSCDNet [39], achieving a mean IoU of 36.83%. We observed that the “object (traffic)” and “object (other)” labels in PSCD often had inconsistent or infrequent annotations, contributing to the relatively lower mIoU. Finally, on the SYSU-CD dataset (Tab. 3), which consists of satellite imagery, ViewDelta achieves state-of-the-art performance with an IoU of 67.18% and an F1 score of 80.37%, outperforming all compared methods on these metrics. These results demonstrate consistent improvements across datasets, underscoring the robustness of ViewDelta. We attribute this performance to the model’s multi-domain training, which enables it to generalize effectively across different change detection domains and scale more easily than specialized methods as combinations of datasets can be used to train with.

5.2. Qualitative Evaluation

We show our model results on example image pairs from the test sets of CSeg, PSCD, and SYSU-CD in Fig. 6. All SYSU-CD test images use the text prompt of: “urban development, suburban expansion, pre-construction groundwork, vegetation alteration, road widening, and coastal construction”.

5.3. Limitations

CSeg and PSCD are limited to minor perspective differences, which limits the models generalizability to large perspective changes. However, expanding the dataset to include larger perspective changes is challenging due to the limited availability of the required data in addition to the difficulty in labeling the data. Another limitation is the exponential increase in the number of image tokens required for higher resolution images that may contain small changes. However, this can be mitigated as compute is scaled.

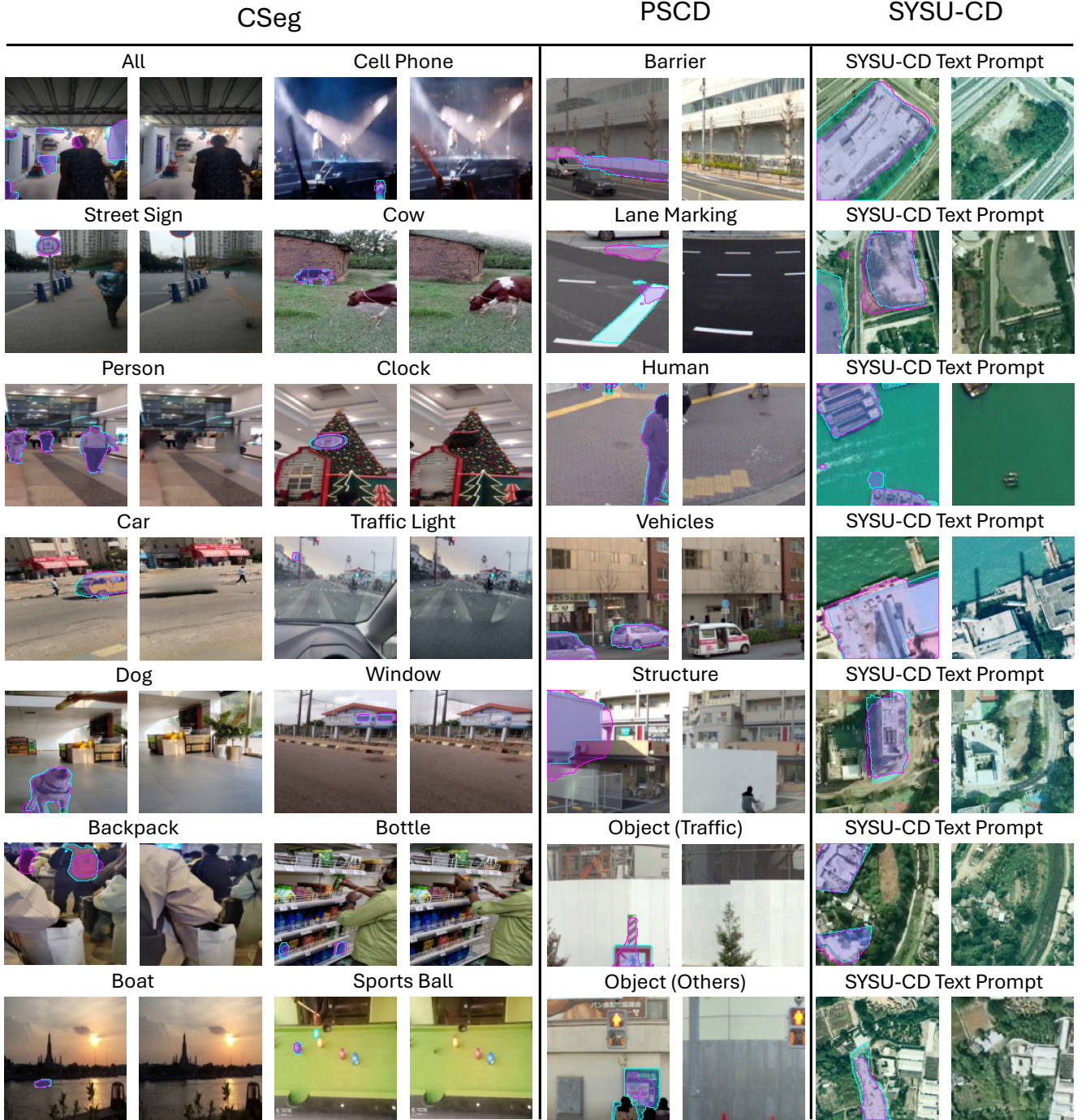


Figure 6. **Qualitative Results:** We show the segmentation **predictions in purple** of our model on the test sets, along with the **ground truth in blue**. All SYSU-CD test images use the text prompt of: “urban development, suburban expansion, pre-construction groundwork, vegetation alteration, road widening, and coastal construction”.

6. Conclusion

We introduce ViewDelta, the first text-prompted change detection model that accepts unaligned images and a text

prompt to output a binary segmentation of changes relevant to the user-provided text. We also release an accompanying dataset, CSeg, comprising 100,311 pairs of images with text prompts and corresponding change detection la-

bels. We demonstrate the effectiveness of ViewDelta both quantitatively and qualitatively on datasets with a wide variety of images including indoor, outdoor, street level, synthetic, and satellite images.

Acknowledgments: Placeholder

References

- [1] Aikaterini Adam, Konstantinos Karantzas, Lazaros Grammatikopoulos, and Torsten Sattler. Has anything changed? 3d change detection by 2d segmentation masks, 2023. [2](#)
- [2] Joshua Ainslie, James Lee-Thorp, Michiel de Jong, Yuri Zemlyanskiy, Federico Lebrón, and Sumit Sanghai. Gqa: Training generalized multi-query transformer models from multi-head checkpoints. *arXiv preprint arXiv:2305.13245*, 2023. [4](#)
- [3] Abdulaziz Amer Aleissae, Amandeep Kumar, Rao Muhammad Anwer, Salman Khan, Hisham Cholakkal, Gui-Song Xia, and Fahad Shabbaz Khan. Transformers in remote sensing: A survey. *Remote Sensing*, 15(7):1860, 2023. [2](#)
- [4] Ting Bai, Le Wang, Dameng Yin, Kaimin Sun, Yepi Chen, Wenzhuo Li, and Deren Li. Deep learning for change detection in remote sensing: a review. *Geo-spatial Information Science*, 26(3):262–288, 2023. [1](#)
- [5] Gong Cheng, Ceyuan Yang, Xiwen Yao, Lei Guo, and Junwei Han. When deep learning meets metric learning: Remote sensing image scene classification via learning discriminative cnns. *IEEE Transactions on Geoscience and Remote Sensing*, 56:2811–2821, 2018. [7](#)
- [6] Guangliang Cheng, Yunmeng Huang, Xiangtai Li, Shuchang Lyu, Zhaoyang Xu, Hongbo Zhao, Qi Zhao, and Shiming Xiang. Change detection methods for remote sensing in the last decade: A comprehensive review. *Remote Sensing*, 16(13):2355, 2024. [1, 7](#)
- [7] Antonio Criminisi, Patrick Pérez, and Kentaro Toyama. Region filling and object removal by exemplar-based image inpainting. *IEEE Transactions on image processing*, 13(9):1200–1212, 2004. [7](#)
- [8] Rodrigo Caye Daudt, Bertrand Le Saux, and Alexandre Boulch. Fully convolutional siamese networks for change detection, 2018. [7](#)
- [9] Lei Ding, Haitao Guo, Sicong Liu, Lichao Mou, Jing Zhang, and Lorenzo Bruzzone. Bi-temporal semantic reasoning for the semantic change detection in hr remote sensing images. *IEEE Transactions on Geoscience and Remote Sensing*, 60:1–14, 2022. [2](#)
- [10] Abhimanyu Dubey, Abhinav Jauhri, Abhinav Pandey, Abhishek Kadian, Ahmad Al-Dahle, Aiesha Letman, Akhil Mathur, Alan Schelten, Amy Yang, Angela Fan, et al. The llama 3 herd of models. *arXiv preprint arXiv:2407.21783*, 2024. [4](#)
- [11] Stefan Elfving, Eiji Uchibe, and Kenji Doya. Sigmoid-weighted linear units for neural network function approximation in reinforcement learning. *Neural networks*, 107:3–11, 2018. [4](#)
- [12] Zhihang Fu, Yaowu Chen, Hongwei Yong, Rongxin Jiang, Lei Zhang, and Xian-Sheng Hua. Foreground gating and background refining network for surveillance object detection. *IEEE Transactions on Image Processing*, PP:1–1, 2019. [1](#)
- [13] Samir Yitzhak Gadre, Gabriel Ilharco, Alex Fang, Jonathan Hayase, Georgios Smyrnis, Thao Nguyen, Ryan Marten, Mitchell Wortsman, Dhruva Ghosh, Jieyu Zhang, et al. Datacomp: In search of the next generation of multimodal datasets. *Advances in Neural Information Processing Systems*, 36, 2024. [3](#)
- [14] Andrew Gonzalez, Jonathan M Chase, and Mary I O’Connor. A framework for the detection and attribution of biodiversity change. *Philosophical Transactions of the Royal Society B*, 378(1881):20220182, 2023. [2](#)
- [15] Ebrahim Hamidi, Brad G Peter, David F Muñoz, Hamed Moftakhari, and Hamid Moradkhani. Fast flood extent monitoring with sar change detection using google earth engine. *IEEE Transactions on Geoscience and Remote Sensing*, 61:1–19, 2023. [2](#)
- [16] Ji Han, Xing Meng, Xiang Zhou, Bailu Yi, Min Liu, and Wei-Ning Xiang. A long-term analysis of urbanization process, landscape change, and carbon sources and sinks: A case study in china’s yangtze river delta region. *Journal of Cleaner Production*, 141:1040–1050, 2017. [1](#)
- [17] Jiaya Jia and Chi-Keung Tang. Image repairing: Robust image synthesis by adaptive nd tensor voting. In *2003 IEEE Computer Society Conference on Computer Vision and Pattern Recognition, 2003. Proceedings.*, pages I–I. IEEE, 2003. [7](#)
- [18] Huiwei Jiang, Min Peng, Yuanjun Zhong, Haofeng Xie, Zemin Hao, Jingming Lin, Xiaoli Ma, and Xiangyun Hu. A survey on deep learning-based change detection from high-resolution remote sensing images. *Remote Sensing*, 14(7):1552, 2022. [1](#)
- [19] Qing Jiang, Feng Li, Zhaoyang Zeng, Tianhe Ren, Shilong Liu, and Lei Zhang. T-rex2: Towards generic object detection via text-visual prompt synergy, 2024. [5, 6](#)
- [20] Diederik P Kingma. Adam: A method for stochastic optimization. *arXiv preprint arXiv:1412.6980*, 2014. [5](#)
- [21] Alexander Kirillov, Eric Mintun, Nikhila Ravi, Hanzi Mao, Chloe Rolland, Laura Gustafson, Tete Xiao, Spencer Whitehead, Alexander C. Berg, Wan-Yen Lo, Piotr Dollár, and Ross Girshick. Segment anything. *arXiv:2304.02643*, 2023. [5, 6](#)
- [22] Tsung-Yi Lin, Michael Maire, Serge Belongie, James Hays, Pietro Perona, Deva Ramanan, Piotr Dollár, and C Lawrence Zitnick. Microsoft coco: Common objects in context. In *Computer Vision–ECCV 2014: 13th European Conference, Zurich, Switzerland, September 6–12, 2014, Proceedings, Part V 13*, pages 740–755. Springer, 2014. [6](#)
- [23] Haotian Liu, Chunyuan Li, Yuheng Li, and Yong Jae Lee. Improved baselines with visual instruction tuning, 2023. [6](#)
- [24] Haotian Liu, Chunyuan Li, Qingyang Wu, and Yong Jae Lee. Visual instruction tuning, 2023.
- [25] Haotian Liu, Chunyuan Li, Yuheng Li, Bo Li, Yuanhan Zhang, Sheng Shen, and Yong Jae Lee. Llava-next: Improved reasoning, ocr, and world knowledge, 2024. [6](#)
- [26] Ze Liu, Yutong Lin, Yue Cao, Han Hu, Yixuan Wei, Zheng Zhang, Stephen Lin, and Baining Guo. Swin transformer:

- Hierarchical vision transformer using shifted windows. In *Proceedings of the IEEE/CVF International Conference on Computer Vision (ICCV)*, pages 10012–10022, 2021. 3
- [27] Ziqi Lu, Jianbo Ye, and John Leonard. 3dgs-cd: 3d gaussian splatting-based change detection for physical object rearrangement, 2024. 2
- [28] Timo Lüddecke and Alexander Ecker. Image segmentation using text and image prompts. In *Proceedings of the IEEE/CVF conference on computer vision and pattern recognition*, pages 7086–7096, 2022. 2
- [29] Huaishao Luo, Junwei Bao, Youzheng Wu, Xiaodong He, and Tianrui Li. Segclip: Patch aggregation with learnable centers for open-vocabulary semantic segmentation. In *International Conference on Machine Learning*, pages 23033–23044. PMLR, 2023. 2
- [30] Tim Newbold, Lawrence N Hudson, Samantha LL Hill, Sara Contu, Igor Lysenko, Rebecca A Senior, Luca Börger, Dominic J Bennett, Argyrios Choimes, Ben Collen, et al. Global effects of land use on local terrestrial biodiversity. *Nature*, 520(7545):45–50, 2015. 1
- [31] Maria Papadomanolaki, Sagar Verma, Maria Vakalopoulou, Siddharth Gupta, and Konstantinos Karantzas. Detecting urban changes with recurrent neural networks from multi-temporal sentinel-2 data, 2019. 7
- [32] Jin-Man Park, Jae-hyuk Jang, Sahng-Min Yoo, Sun-Kyung Lee, Ue-hwan Kim, and Jong-Hwan Kim. Changesim: Towards end-to-end online scene change detection in industrial indoor environments. In *2021 IEEE/RSJ International Conference on Intelligent Robots and Systems (IROS)*. IEEE, 2021. 2
- [33] Alec Radford, Jong Wook Kim, Chris Hallacy, Aditya Ramesh, Gabriel Goh, Sandhini Agarwal, Girish Sastry, Amanda Askell, Pamela Mishkin, Jack Clark, et al. Learning transferable visual models from natural language supervision. In *International conference on machine learning*, pages 8748–8763. PMLR, 2021. 3
- [34] Nikhila Ravi, Valentin Gabeur, Yuan-Ting Hu, Ronghang Hu, Chaitanya Ryali, Tengyu Ma, Haitham Khedr, Roman Rädle, Chloe Rolland, Laura Gustafson, et al. Sam 2: Segment anything in images and videos. *arXiv preprint arXiv:2408.00714*, 2024. 5
- [35] Tianhe Ren, Qing Jiang, Shilong Liu, Zhaoyang Zeng, Wenlong Liu, Han Gao, Hongjie Huang, Zhengyu Ma, Xiaoke Jiang, Yihao Chen, Yuda Xiong, Hao Zhang, Feng Li, Peijun Tang, Kent Yu, and Lei Zhang. Grounding dino 1.5: Advance the “edge” of open-set object detection, 2024. 5, 6
- [36] Tianhe Ren, Shilong Liu, Ailing Zeng, Jing Lin, Kunchang Li, He Cao, Jiayu Chen, Xinyu Huang, Yukang Chen, Feng Yan, Zhaoyang Zeng, Hao Zhang, Feng Li, Jie Yang, Hongyang Li, Qing Jiang, and Lei Zhang. Grounded sam: Assembling open-world models for diverse visual tasks, 2024. 5, 6
- [37] Ragav Sachdeva and Andrew Zisserman. The change you want to see (now in 3d). In *Proceedings of the IEEE/CVF International Conference on Computer Vision*, pages 2060–2069, 2023. 2, 5
- [38] Keiko Saito, Robin JS Spence, Christopher Going, and Michael Markus. Using high-resolution satellite images for post-earthquake building damage assessment: a study following the 26 january 2001 gujarat earthquake. *Earthquake spectra*, 20(1):145–169, 2004. 1
- [39] Ken Sakurada, Mikiya Shibuya, and Weimin Wang. Weakly supervised silhouette-based semantic scene change detection, 2022. 2, 7
- [40] Qian Shi, Mengxi Liu, Shengchen Li, Xiaoping Liu, Fei Wang, and Liangpei Zhang. A deeply supervised attention metric-based network and an open aerial image dataset for remote sensing change detection. *IEEE Transactions on Geoscience and Remote Sensing*, pages 1–16, 2021. 2, 7
- [41] Wenzhong Shi, Min Zhang, Rui Zhang, Shanxiong Chen, and Zhao Zhan. Change detection based on artificial intelligence: State-of-the-art and challenges. *Remote Sensing*, 12(10):1688, 2020. 1
- [42] Ashbindu Singh. Review article digital change detection techniques using remotely-sensed data. *International journal of remote sensing*, 10(6):989–1003, 1989. 1
- [43] Jian Song, Hongruixuan Chen, and Naoto Yokoya. Syntheworld: A large-scale synthetic dataset for land cover mapping and building change detection. In *Proceedings of the IEEE/CVF Winter Conference on Applications of Computer Vision (WACV)*, pages 8287–8296, 2024. 2
- [44] Jérémie Sublime and Ekaterina Kalinicheva. Automatic post-disaster damage mapping using deep-learning techniques for change detection: Case study of the tohoku tsunami. *Remote Sensing*, 11(9):1123, 2019. 1
- [45] Quan Sun, Yuxin Fang, Ledell Wu, Xinlong Wang, and Yue Cao. Eva-clip: Improved training techniques for clip at scale. *arXiv preprint arXiv:2303.15389*, 2023. 3
- [46] Yanjun Sun, Yue Qiu, Mariia Khan, Fumiya Matsuzawa, and Kenji Iwata. The stvchron dataset: Towards continuous change recognition in time. In *Proceedings of the IEEE/CVF Conference on Computer Vision and Pattern Recognition (CVPR)*, pages 14111–14120, 2024. 2
- [47] Roman Suvorov, Elizaveta Logacheva, Anton Mashikhin, Anastasia Remizova, Arsenii Ashukha, Aleksei Silvestrov, Naejin Kong, Harshith Goka, Kiwoong Park, and Victor Lempitsky. Resolution-robust large mask inpainting with fourier convolutions. *arXiv preprint arXiv:2109.07161*, 2021. 5
- [48] Gemini Team, Rohan Anil, Sebastian Borgeaud, Jean-Baptiste Alayrac, Jiahui Yu, Radu Soricut, Johan Schalkwyk, Andrew M Dai, Anja Hauth, Katie Millican, et al. Gemini: a family of highly capable multimodal models. *arXiv preprint arXiv:2312.11805*, 2023. 5, 6
- [49] Wenhai Wang, Enze Xie, Xiang Li, Deng-Ping Fan, Kaitao Song, Ding Liang, Tong Lu, Ping Luo, and Ling Shao. Pyramid vision transformer: A versatile backbone for dense prediction without convolutions. In *Proceedings of the IEEE/CVF international conference on computer vision*, pages 568–578, 2021. 3
- [50] Chuyi Wu, Feng Zhang, Junshi Xia, Yichen Xu, Guoqing Li, Jibo Xie, Zhenhong Du, and Renyi Liu. Building damage detection using u-net with attention mechanism from pre-and post-disaster remote sensing datasets. *Remote Sensing*, 13(5):905, 2021. 1

- [51] Enze Xie, Wenhai Wang, Zhiding Yu, Anima Anandkumar, Jose M Alvarez, and Ping Luo. Segformer: Simple and efficient design for semantic segmentation with transformers. *Advances in neural information processing systems*, 34: 12077–12090, 2021. [3](#)
- [52] Kunping Yang, Gui-Song Xia, Zicheng Liu, Bo Du, Wen Yang, Marcello Pelillo, and Liangpei Zhang. Semantic change detection with asymmetric siamese networks, 2021. [2](#)
- [53] Shuai Yi, Hongsheng Li, and Xiaogang Wang. Pedestrian behavior modeling from stationary crowds with applications to intelligent surveillance. *Trans. Img. Proc.*, 25(9):4354–4368, 2016. [1](#)
- [54] Xiaohua Zhai, Basil Mustafa, Alexander Kolesnikov, and Lucas Beyer. Sigmoid loss for language image pre-training. In *Proceedings of the IEEE/CVF International Conference on Computer Vision*, pages 11975–11986, 2023. [3](#)
- [55] Hang Zhao, Xavier Puig, Bolei Zhou, Sanja Fidler, and Antonio Torralba. Open vocabulary scene parsing. In *Proceedings of the IEEE International Conference on Computer Vision*, pages 2002–2010, 2017. [2](#)
- [56] Qiqi Zhu, Xi Guo, Ziqi Li, and Deren Li. A review of multi-class change detection for satellite remote sensing imagery. *Geo-spatial Information Science*, 27(1):1–15, 2024. [2](#)